Experimental study and associated numerical simulation of horizontally-connected precast shear wall assembly

Experimental study and associated numerical simulation of horizontally-connected precast shear wall assembly

Jian Sun[1], Hongxing Qiu[1,*], Yong Lu[2]

[1] *Key Laboratory of Concrete and Prestressed Concrete Structures of Ministry of Education, Southeast University, Nanjing, China;*

[2] *Institute for Infrastructure and Environment, School of Engineering, The University of Edinburgh, Edinburgh, UK*

SUMMARY

This paper is concerned about precast reinforced concrete shear walls and the methods of assembling shear wall panels to form a reliable load transfer system. An assembling method is proposed using dry connection through a horizontal steel connector (H-connector) and high strength bolts. To investigate the effectiveness and the design of such a connection method, three wall-connector assembly specimens with different connection details have been constructed and tested under monotonic loading while subjected to a constant vertical compression. The test results provided comprehensive data regarding the progressive transition of the load transfer mechanisms and showed that the performance of the shear wall assembly was generally satisfactory in terms of ensuring the full development of the shear wall strength and ductility. To assist in the interpretation of the experimental results and enable further parametric analysis, a detailed finite element model has been developed with incorporation of the main load transfer mechanisms, in addition to the description of the nonlinear behaviour of the shear wall. The FE model has been verified to represent well the actual behaviour of the shear wall assembly and it has provided further insight into the occurrence of slippage at the connection, the development of the bearing resistance of the bolts and the compression load transfer through contact in the later stage of the response.

Keywords: precast shear wall; horizontal connection; steel connector; high strength bolts; load transfer mechanisms; finite element analysis

*Correspondence to: Hongxing Qiu, Key Laboratory of Concrete and Prestressed Concrete Structures of Ministry of Education, Southeast University, Nanjing 210096, China.
Email: qiuhx@seu.edu.cn

1 Introduction

Precast reinforced concrete (RC) construction is common in many parts of the world. Typically, it involves the mass production of repetitive and often standardized units, namely columns, beams, floor and roof elements, and wall panels. Advantages of precast construction include less labour cost and shorter construction time, as well as better quality control. Higher concrete strength is also more achievable under factory conditions. Precast RC structures with special detailing and treatment at the connections are also popular in seismic regions. However, comparing with other precast components, precast RC shear wall is relatively under-developed, and this has become a bottleneck problem in the precast construction of medium to high rise buildings in seismic regions.

Shear wall is an essential structural member to resist lateral seismic loading in high rise buildings (Lu and Yang, 2015). Due to the need of maintaining high lateral stiffness and resistance, precast shear wall poses particular challenges to the assembling techniques. Although there has not been a well-established approach, researchers worldwide have carried out investigations on various kinds of prefabricated concrete shear wall systems.

A series of experimental and analytical studies were performed on the unbonded post-tensioned (UPT) precast concrete wall system (Kurama *et al*., 1999; Perez *et al*., 2007; Henry *et al*., 2012; Perez *et al*., 2013). The UPT system is normally constructed by post-tensioning precast wall panels across horizontal joints at the floor levels using UPT steel, whereas the vertical joints between the adjacent wall panels employ discontinuous ductile connectors to transfer the vertical shear force and dissipate energy under seismic loading. Further studies along this line looked into enhancing the energy-dissipating capacity of the UPT walls using a hybrid method with a combination of mild steel and high-strength UPT steel (Kurama, 2002; Smith *et al*., 2013; Belleri *et al*., 2014). The main advantages of this system include the potential ability to minimize the residual drifts and hence reduce the structural damage. However, the use of vertical post-tensioning in the UPT precast concrete wall system tends to demand thicker walls so as to accommodate the required high

compressive force capacity, and special confining reinforcement such as spiral reinforcement may also be required at the edges of the wall.

Mechanical bolted connections are also used to tie together precast concrete panel elements (Shemie, 1973; Pall *et al*., 1980; Pekau and Hum, 1991). The connections are generally composed of steel inserts embedded in the concrete panel by stud-welded anchor bars. During erection two such inserts are firstly held in place adjacent to each, and then a connecting plate is bolted onto the embedded inserts to complete the connection. Bora *et al.* (2007) used a slotted-bolted (SB) connection to join hollow-core panel with floor to form a precast concrete shear wall system. The SB connection allows certain slippage between the plates under a seismic force, and this enables an elastic-plastic response of the connection and thus a high energy-dissipating capacity. It was also found that the SB connected shear wall system was ductile. The precast concrete shear wall system employing SB connectors to join the hollow-core panel with the floor is generally suitable for low-rise commercial and industrial buildings. In a similar manner, steel connectors in various arrangements have been adopted in beam-to-column connections in a precast moment resisting frame system (Choi *et al*. 2013).

The horizontal connection between adjacent precast shear wall panels may also be achieved using “wet” methods, for instance by inserting the extended rebar at the top face of the below panel into the preformed hole at the bottom of the above panel and filling the preformed hole with fresh cementitious grout (Jiang *et al*. 2011), or by sleeve-mortar splicing together with cast-in-situ concrete (Qian *et al*. 2011). “Wet” methods have also found new applications in precast concrete frame-wall systems (Negro *et al*. 2013; Bournas *et al*. 2013). However, these types of assembling procedures all require some cast-in-situ work, which reduces the construction efficiency to some extent.

In a prefabricated RC sandwich wall system (Pavese and Bournas, 2011), the sandwich panels are connected with the foundation using starter bars and sprayed concrete layers. It was found that such a wall system exhibited satisfactory seismic performance. Similar assembling methods have also been investigated by Zhang *et al*. (2011) and Wang *et al*. (2015).

In summary, the existing assembling methods for precast shear walls may be classified broadly into the following three types, a) unbonded post-tensioned, b) mechanically bolted, and c) direct splicing of steel bars combined with cast-in-situ concrete.

In this paper we propose an innovative precast RC shear wall system in an effort to maximize the structural integrity in resisting seismic loads, and at the same time maintaining desirable assembling efficiency. The general design concept will be explained first. An experimental programme on three specimens under the same design framework but with variation in the connection details is presented next. The experimental results are then analyzed and discussed. This is followed by a finite element analysis of the test specimens for the purpose of validating the FE model and subsequently enhanced interpretation of the experimental observations using the FE results. In the last part of the paper, the general working mechanisms of the particular bolted connections in the proposed wall assembly are discussed.

2 The proposed precast shear wall system

2.1 Brief description

The proposed precast concrete shear wall system utilizes horizontal steel connector (H-connector) and high strength bolts to connect the adjacent shear wall panels and floor panels together to form an integrated lateral load-resisting structural system. The horizontal connection serves to transfer gravity loads and lateral earthquake and wind loads through the shear wall segments to the base foundation. The concept is illustrated in Figure 1.

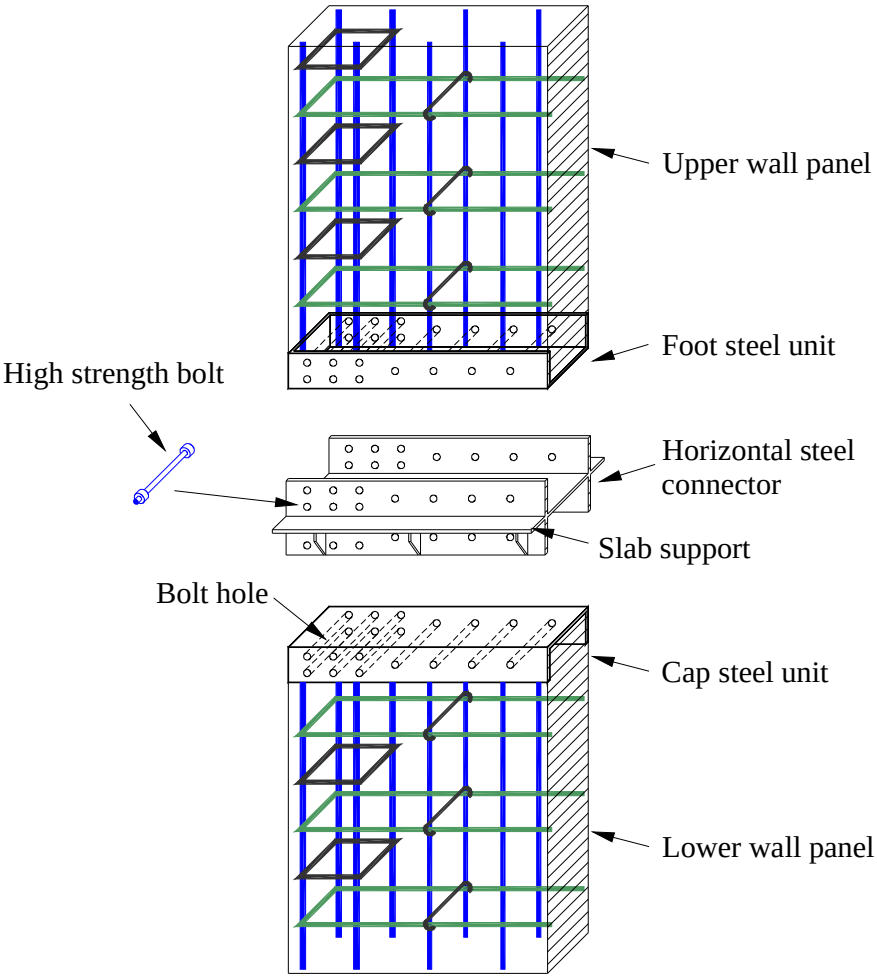

Figure 1 Schematic of the system concept

2.2 Functions of connecting components

A complete horizontal connection is made up of three components. The functions of these connecting components are explained in detail as follows.

(1) Horizontal steel connector (H-connector). The H-connector is the central piece of the connection and it is an H-shaped steel segment. As shown in Figure 1, it may be made to include extended studs on the two sides to provide floor slab supporting. A basic function of the H-connector is to transfer external loads from the above shear walls (and floor slabs if fitted) to the shear walls below.

(2) Top / bottom steel units in shear wall panel. These units are welded channel sections and are cast onto the shear wall panel. To ensure their structural integration with the shear wall panel, vertical steel bars are welded to their inner side before casting. Bolt holes are

easily positioned with precision through the side plates of these units, allowing better controlled assembling of the bolted connection. Furthermore, these channel sections also act as confinement which helps ensure that failure does not occur in concrete within the connection.

(3) High strength bolts. As shown in Figure 1, high strength bolts are used to fix the precast concrete walls into H-connector. The pre-tensioning force in the bolts, which can be controlled by a calibrated torque wrench, generates normal pressure on the contact interface between the connector and the adjoining shear wall panels, and subsequently results in frictional resistance which is a main mechanism of the lateral load transfer through the connection. This is elaborated further in the section that follows.

2.3 General working mechanisms of the bolted connection

It is well known that the load-transferring mechanisms of a bolted connection before and after the occurrence of sliding are different (Ju *et al*., 2004). Before sliding, the external load is transferred just by the frictional action. When sliding occurs, the external load is transferred by both frictional action and bolt bearing action.

In the present shear wall horizontal connection, the transfer of the lateral load is similarly achieved via friction before sliding occurs, and subsequently by a combination of friction and the bolt bearing actions. Because the connection is subjected to bending as well as lateral shear, when sliding develops it will be associated with rotation. Consequently on the compressive side any initial gap between the wall panel and the H-connector may close and this will contribute to some extent in the transfer of the lateral load. The transfer of load through closure of the gap brings in an uncertain factor in terms of the real connection behaviour and should be noted when it comes to comparing the experimental results.

If the relative positions of the bolts to the bolt holes in the wall are uniform, the transition from the initial friction-only stage to the combined friction and bolt bearing stage would imply a step increase of the deformation. However, in reality the bolts can be expected to get engaged one by one gradually, resulting in a nonlinear transition. This will be illustrated and discussed later with the experimental results in conjunction with finite element analysis.

3 Experimental investigation

3.1 Test setup and specimen design

A proof-of-concept testing study was carried out prior to the finalized experimental programme reported in this paper. The preliminary test results (Sun *et al*., 2015) confirmed that the general idea of assembling shear wall units through bolted H-connectors was feasible and the connection could provide sufficient strength and rigidity. On this basis, three test specimens, denoted as WH-r1, WH-r2, and WH-r3 were constructed and tested under monotonic loading to study comprehensively the lateral load response of the connected shear wall. The three specimens had identical wall design but they differed from each other in the connection details, as explained later in this section.

To simplify the specimen design and the test setup, while maintaining realistic connection details, each test specimen assembly is comprised of one main shear wall panel, a short wall segment which is cast together with a strong base girder, and a full H-connector that connects the wall panel to the short wall segment on top of the base support.

In the design of the main wall panel, to be generally representative we chose a typical reinforcement scheme instead of specifying a design strength. The vertical reinforcement had a reinforcement ratio of 0.42% (well within a normal range of 0.2-1%), and the horizontal reinforcement was 0.7% so as to ensure that no premature shear failure would occur in the test specimens. With a typical concrete strength chosen to be C35, it was calculated that the achieved design shear strength of the walls was approximately 195 kN. The design of the bolts was made so that the strength of the bolted connection exceeded the shear strength of the wall by a sufficient margin of safety. A checking calculation found that the strengths of the bolted horizontal connections, assuming no damage to the H-connector, were approximately 600kN, 330kN, and 600kN for specimens WH-r1, WH-r2 and WH-r3, respectively.

Figure 2 shows a schematic of the specimen assembly and the details of individual components. The components in each test assembly are described in more detail as follows.

(1) Precast RC shear wall. This part consists of the main wall panel, a steel footing unit which is cast into the bottom of the wall panel. At the top of the wall panel a beam is also cast

with the wall panel for the loading purpose. The configurations of the wall panels and loading beams in the three specimens are the same, as shown in Figure 2(a). Note that in the figure the steel bars are denoted as A6 and C10, where A6 represents Grade HPB300 (270 MPa) steel bars of 6 mm in diameter, and C10 represents HRB400 (360 MPa) steel bars of 10 mm in diameter.

(2) H-connector. The H-shaped horizontal connector is welded using a web plate of 6 mm thick, while the two flange plates have thickness (t_2) which is one of the variable parameters being investigated.

(3) Foundation beam. The foundation beam is intentionally designed to be strong enough to allow re-use in the three test specimens. The steel cap unit set on the foundation beam is welded using steel plates of 16 mm thick, as shown in Figure 2(a).

(4) Bolts connecting the shear wall panel with the H-connector. These bolts are made of Grade 10.9s bolts with a nominal yield strength of 900 MPa and a diameter (d) which varies from 12 to 16 mm in different specimens. The pre-tensioning force is also one of the test parameters.

(5) Bolts connecting the above wall-connector assembly to the short wall on the foundation beam. These bolts are deliberately made very strong using M22 bolts with a large pre-tensioning force (190 kN) to effectively enable a fixed transition between the H-connector and the foundation beam.

The diameter of the bolt holes (d_0) is made equal to the diameter of the bolts plus a 2 mm margin. Once the wall panel and H-connector are brought together with the foundation beam, bolts are placed and then tightened to the desired pre-positioning levels to complete the horizontal connection and form the specimen.

The test variable parameters among the three specimens WH-r1, WH-r2 and WH-r3 were in the details of the connections, including the thickness of side plate in the footing unit (t_1), the thickness of flange plate of the H-connector (t_2), and the nominal diameter of bolts and the pre-tension force.

Table 1 summarises the values of these parameters in the three different specimens.

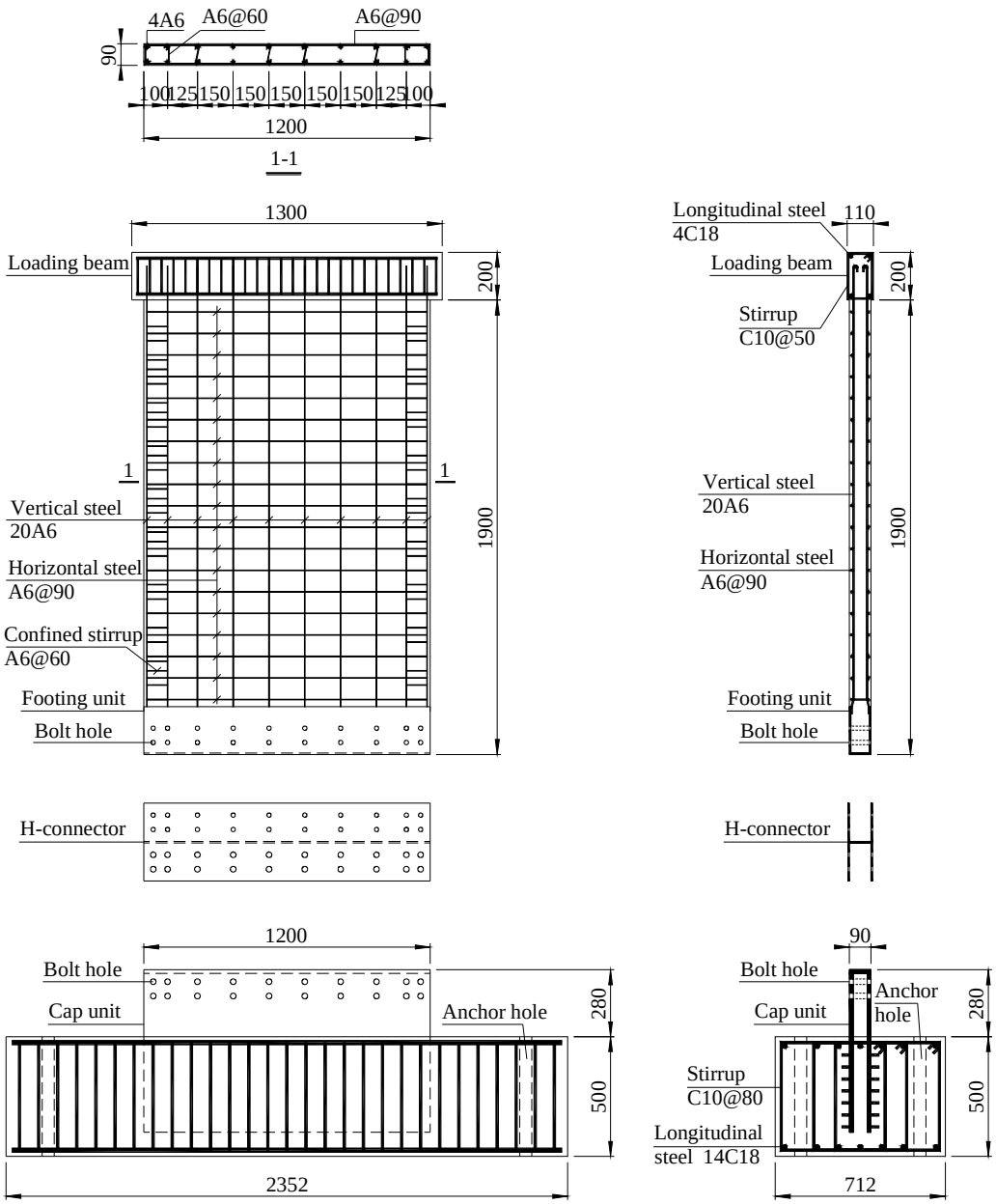

(a) Components of the test assembly and details of the wall panel

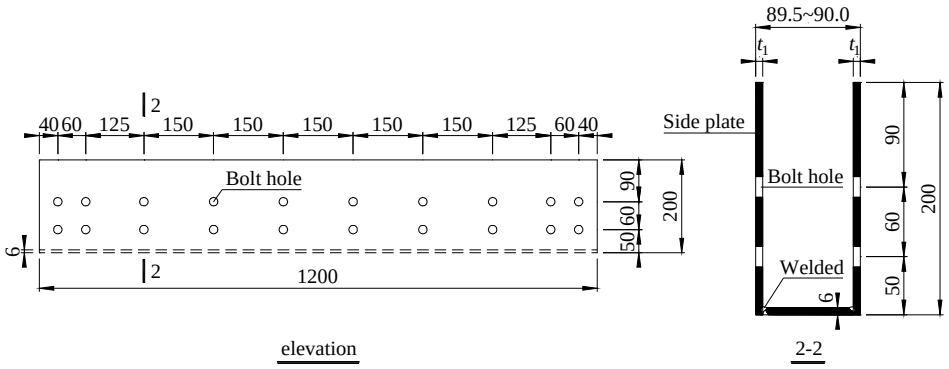

(b) Details of the footing unit

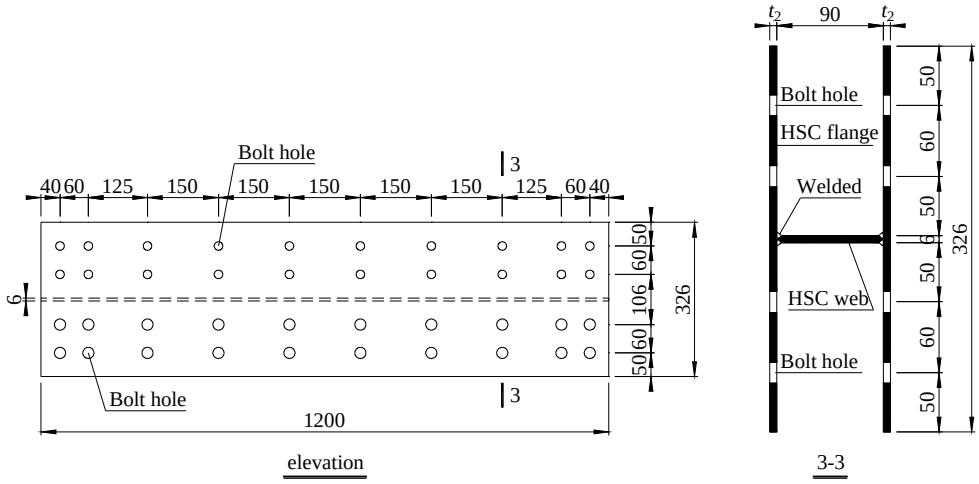

(c) Details of the H-connector

Figure 2 Configuration of the specimens (Unit: mm)

Table 1 Variable parameters in the three test specimens

Specimens	Parameters			
	High strength bolts		Thickness of footing unit	Thickness of H-connector flange
	Diameter (mm)	Pre-tension (kN)	t_1 (mm)	t_2 (mm)
WH-r1	16	100	3	6
WH-r2	12	55	6	6
WH-r3	16	100	6	3

3.2 Material properties

Six standard concrete cubes (150 mm) were prepared during casting of the specimens, and were then cured under the same condition as the test specimens. These cubes were tested during the experiment period for the compressive strength of the concrete. The average compressive strength was found to be 37.4 MPa. Three sample coupons for each type of steel bars and steel plates were also prepared and these were tested under tensile loading to obtain the strength properties. The measured yield strength (f_y) and peak strength (f_u) of the steel bars and steel plates are summarized in Table 2.

Table 2 Measured material property

Material	Yield strength (MPa)	Tensile strength (MPa)
6-mm (A6) reinforcing steel bar	362	530
3-mm-thick steel plate	296	350
6-mm-thick steel plate	350	441

3.3 Loading scheme

All specimens were tested with a horizontal monotonic load to failure. A constant vertical compression force, which represents the gravity load transmitted from the upper part of the shear wall in a building structure, was maintained during each test. Figure 3 shows schematically the loading setup.

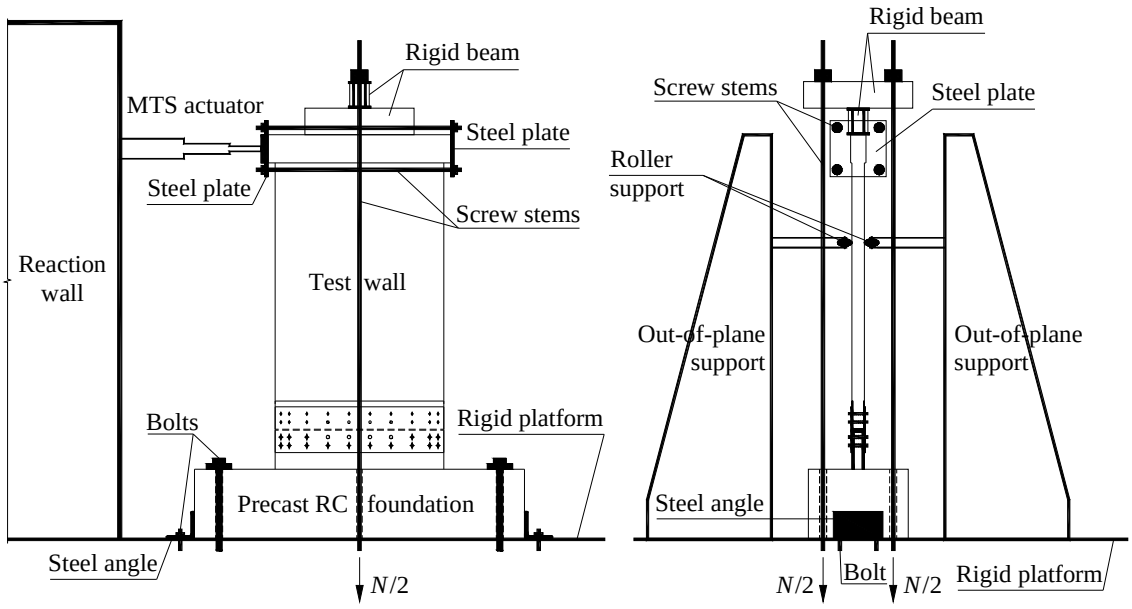

(a) Front elevation (b) Side elevation

(c) Photograph

Figure 3 Loading apparatus

The vertical force was predetermined as 492 kN giving rise to an axial compression ratio of 0.16, and it was applied on the top loading beam by two hydraulic jacks.

The horizontal load was applied on the loading beam by a MTS actuator which was mounted on a reaction wall. The loading was progressively applied in a displacement-controlled manner, with a loading rhythm of 0.5 mm per minute, as follows: at the early stage, the displacement step interval was set at 0.5 mm or 1 mm until the top displacement reached 10 mm; the step interval was then increased to 1 mm or 2 mm until the top displacement reached 30 mm; after that the step interval was further increased to 5 mm until the specimen failed.

3.4 Measurement scheme

The measurement scheme is illustrated in Figure 4. The main measurements include the following:

i) Lateral load and lateral displacement at the top of the wall assembly. The lateral load was measured by a load cell attached to the MTS actuator head, and the lateral displacement was measured by a displacement transducer.

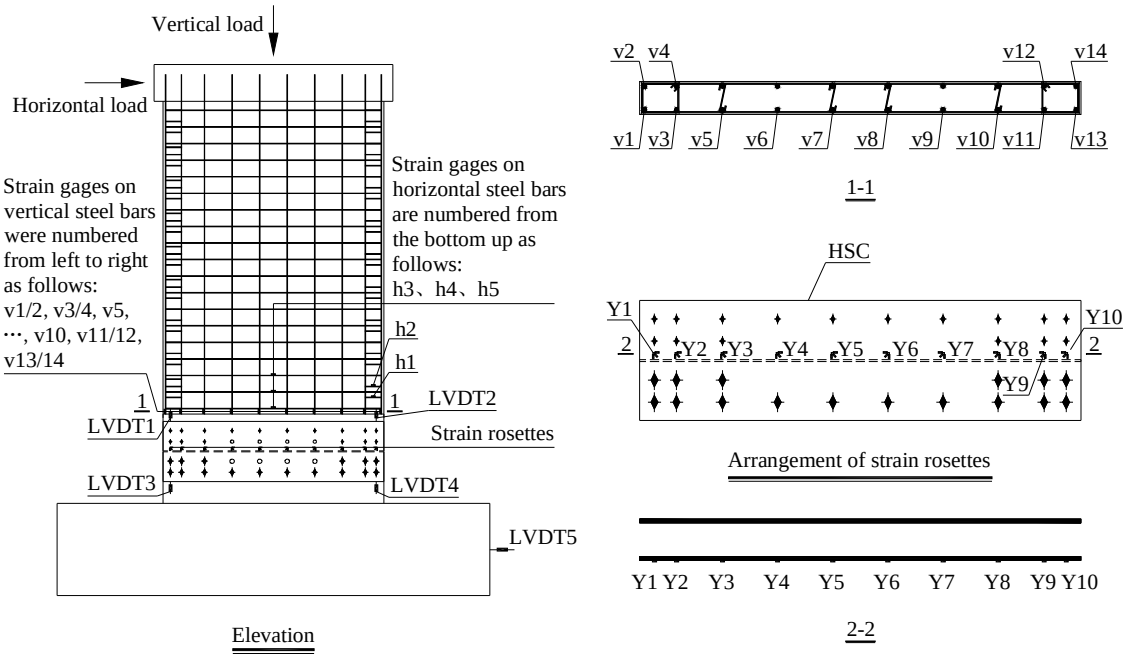

Figure 4 Measurement scheme

ii) Strains in the H-connector. 10 strain rosettes (Y1 to Y10) were installed on the H-connector to measure its strain state.

iii) Strains in steel bars. A number of strain gauges were installed on part of the vertical and horizontal steel bars to record their strains.

iv) Relative displacement (sliding) between the wall footing and the H-connector. This was measured by 4 displacement meters fixed at both ends of the H-connector and attached to the lower end (footing unit) of the wall.

Furthermore, an additional displacement meter was installed on the foundation beam to monitor any rigid-body translation of the whole specimen.

4 Test results and discussion

4.1 General performance and failure modes

4.1.1 Specimen WH-r1

In specimen WH-r1, the first visible crack occurred when the top displacement reached 4 mm, and the crack appeared horizontally at the bottom of the wall panel on the tension side. When the top displacement increased to 5 mm, the first crack cut through the concrete wall. With increase of the top displacement, a number of new cracks appeared while the existing cracks developed continuously. When the lateral displacement increased to 22 mm, a major inclined crack occurred near the wall bottom and it quickly developed into the compressive zone, while some vertical cracks appeared on the compression side of the wall panel, as shown in Figure 5(a). With further increase of the top displacement to about 30-40 mm, concrete began to spall in the compressive zone. When the top displacement reached 55 mm, concrete started crushing in a large area in the bottom compression zone. At the same time, buckling of longitudinal steel bars within the boundary column of the wall panel took place, exposing the horizontal steel bars. Crushing of concrete and buckling of the steel bars pushed

open the footing bracket, as shown in Figure 5(b). The overall failure mode of specimen WH-r1 is shown in Figure 5(c).

(a) Vertical cracks at compression end (b) Compressive failure (c) Overall failure mode

Figure 5 Damage pattern and failure mode of specimen WH-r1

4.1.2 Specimen WH-r2

The general test phenomena of specimen WH-r2 were largely similar to specimen WH-r1. With increasing top displacement, the specimen successively experienced the following stages of the response: cracking of concrete in the tensile zone of the wall panel; yielding of tension steel; cracking and spalling of concrete at the compression side of the wall panel; and final failure of the specimen. The overall failure mode of the specimen is shown in Figure 6(a). However, the footing bracket of the wall panel in specimen WH-r2 remained generally intact (Figure 6(b)) as opposed to an opening-up in WH-r1. This is attributable to the increased thickness of the steel plate for the footing bracket to 6 mm in WH-r2 from 3 mm in WH-r1.

(a) Overall failure mode (b) Failure state at compression end

Figure 6 Specimen WH-r2

Inspection of the deformations in the bolts after dismounting of the tested specimen revealed that the bolts had been engaged with dowel action, and this indicates that certain slippage occurred at the contact surfaces between the footing unit and the H-connector on both tensile and compressive sides of WH-r2.

4.1.3 Specimen WH-r3

Specimen WH-r3 had a reduced thickness in the H-connector, from 6 mm in the previous two specimens to 3 mm. While the general behaviour and damage pattern in this specimen were similar to the previous two specimens, local buckling occurred in the H-connector in the compressive zone when the top displacement was 24 mm, which was well before the final failure with crushing of concrete in the compressive zone. Figure 7(a) and Figure 7(b) show the failure mode of specimen WH-r3. The buckling region within the H-connector is shown in Figure 7(c). Inspection after the test revealed that the weld between the flange and web steel plates in the H-connector was broken while the local buckling occurred.

The occurrence of the local buckling was a result of the an initial gap between the bottom line of the wall panel (footing) and the H-connector, which was estimated to be about 1.5 mm, in conjunction with the use of a thinner flange thickness in the H-connector. However, as will be shown in the next section, the gap closed immediately after the buckling and then the shear wall bottom came into tight contact with the support beam to continue the transfer of the compressive force in the compression zone.

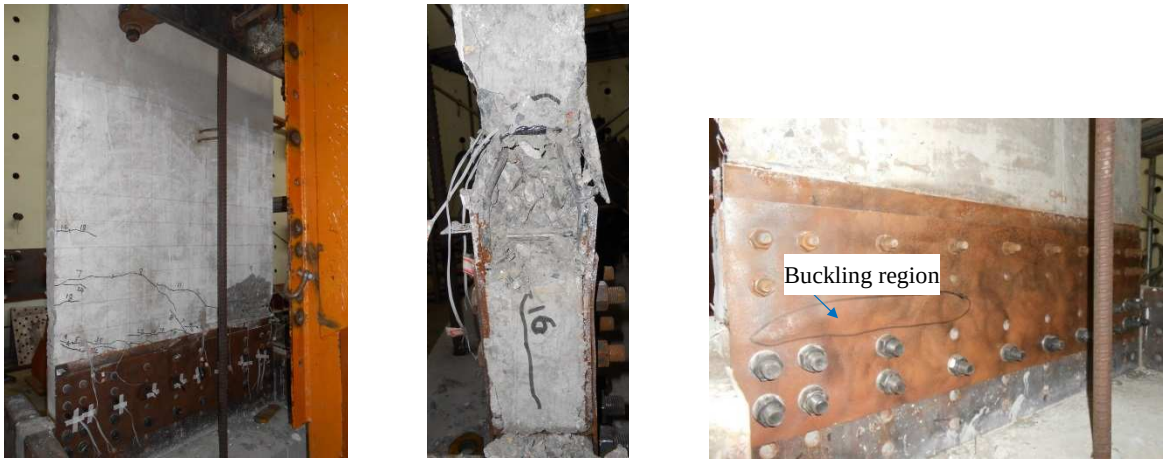

(a) Overall failure mode (b) Failure state at compression end (c) Buckling region

Figure 7 Specimen WH-r3

4.2 Load-displacement relationship and key points

The lateral load versus top displacement curves of the three specimens are shown in Figure 8. Several points representing the key response stages are identified on the curves, including first cracking of concrete, first yielding of tension steel, and first spalling of concrete in the compression zone.

The first visible bending cracks in the three specimens all occurred at a top displacement of about 4 mm. First yielding in the tensile steel bars occurred when the top displacement reached 6.4 mm (WH-r1), 7.5 mm (WH-r2), and 8.8 mm (WH-r3), respectively. The concrete began to spall when the top displacements increased from 30 mm to 35 mm (WH-r1), 18 mm to 20 mm (WH-r2), and 16 mm to 18 mm (WH-r3), respectively.

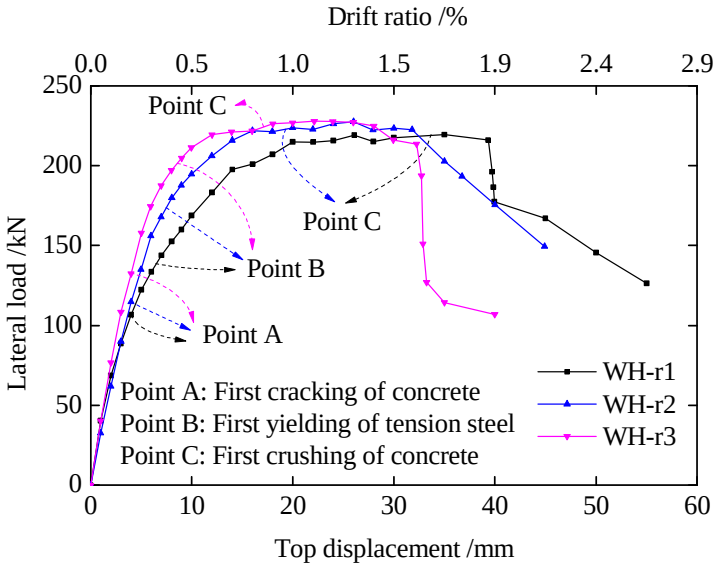

Figure 8 load-displacement curves

Denote the cracking load, yield load, peak load, and failure load as P_{cr}, P_y, P_m, and P_u, and cracking displacement, yield displacement, peak displacement, and ultimate displacement as Δ_{cr}, Δ_y, Δ_m, and Δ_u, respectively. The failure load here is defined at 85% of the maximum load in the post-peak stage of the response, as commonly adopted in earthquake engineering. The determination of the yield load for situations where there is not a clear yielding plateau, different methods may be used to estimate Δ_y and P_y (Park, 1989). In the present study, Δ_y and P_y are determined using the following two methods.

(1) the lateral load and top displacement corresponding to the first yielding of the tension steel farthest from the compression end of the wall panel are taken as yield load (P_y) and yield displacement (Δ_y), respectively.

(2) the yield load (P_y) is firstly calculated as P_y=0.85P_m, and the yield displacement is estimated by extending a line connecting the origin and the point of 0.6P_y on the load-displacement curve to the horizontal line of P=P_y; the displacement of the resulting intersection is assumed as yield displacement (Δ_y).

The results of the above key points are summarized in Table 3. The achieved ductility factors (μ), defined as the ratio between the ultimate displacement to the yield displacement, are also given in the table.

Table 3 Performance indexes of specimens

Specimens	Cracking point			Yield point						Peak point			Failure point			μ	
				(1)			(2)										
	P_{cr}	Δ_{cr}	Δ_{cr}/H	P_y	Δ_y	Δ_y/H	P_y	Δ_y	Δ_y/H	P_m	Δ_m	Δ_m/H	P_u	Δ_u	Δ_u/H	(1)	(2)
WH-r1	106.7	4.0	1/514	137.7	6.4	1/321	186.5	7.2	1/284	219.5	35.0	1/59	186.5	39.9	1/52	6.2	5.5
WH-r2	114.6	4.0	1/514	173.6	7.5	1/275	193.4	6.8	1/303	227.5	26.0	1/79	193.4	36.7	1/56	4.9	5.4
WH-r3	132.4	4.0	1/514	203.5	8.8	1/233	193.5	5.4	1/380	227.8	22.0	1/93	193.7	32.7	1/63	3.7	6.0

Note: H is the wall height measuring from the loading point to the concrete wall bottom; the units of the loads and displacements in this table are kN and mm, respectively.

From Table 3 together with Figure 8 the following observations can be made:

(1) The ultimate bearing capacities (equal to peak loads) of the specimens are close to each other, indicating that the local buckling in the H-connector in specimen WH-r3 did not affect sensibly the resistance capacity of the wall. The three connection schemes are thus deemed to be capable of providing sufficient connection strength so as to allow the full development of the strength of the RC shear wall. It should be kept in mind that the performance with a thinner connector as represented by WH-r3 could be more susceptible to construction uncertainties, especially the gaps at the bottom of the wall; and

(2) Overall the ductility of all the three specimens is good, and the achieved ductility factor is on the order of 5 in all cases. Specimen WH-r3 exhibited a more abrupt final failure process (Figure 9), and this may be related to the reduced integrity of the H-connector due to local buckling

4.3 Strains in steel bars

Figure 9 shows the relationship of strains in the longitudinal (vertical) steel bars across the bottom section to the top displacement for the three specimens. Positive sense indicates tensile strains on the tension side of the section, and negative sense indicates compressive strains on the compression side of the section. It can be seen that initially the whole bottom section was in compression due to the axial load. As the lateral load increased, the section cracked and this led to significant increase of the tensile strains in the tension bars. As the lateral displacement further increased, the neutral axis gradually shifted rightwards, indicating crushing of concrete and hence loss of part of the compression zone. At the failure stage the neutral axis was between the v9 and v10 steel bars (v1 to v9 were all in tension while v10 to v14 were all in compression) in all three specimens. In other words, when the specimens failed the distance from the neutral axis to the tension ends of the precast shear walls was all in the range of 825 mm to 975 mm. The magnitude of tensile strains was much larger than the compressive strains, and this is line with a general flexural failure mode.

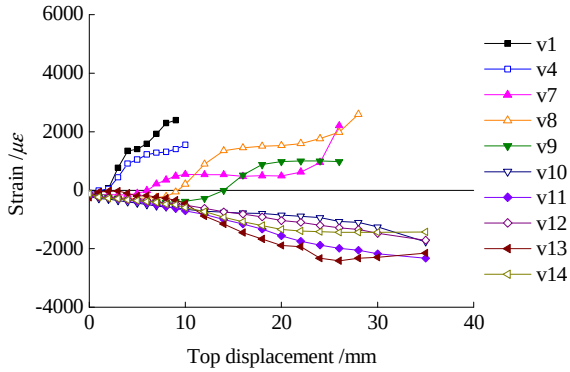

(a) Specimen WH-r1

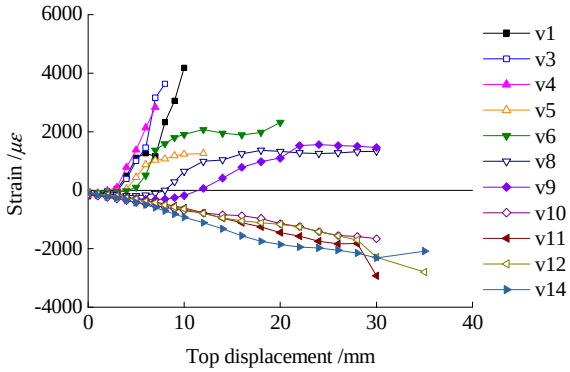

(b) Specimen WH-r2

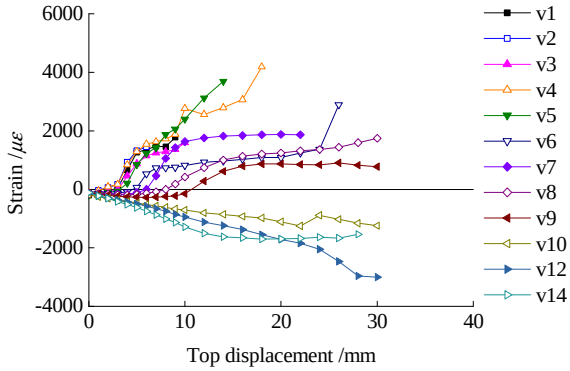

(c) Specimen WH-r3

Figure 9 Strains in vertical steel bars-top displacement curves

4.4 Strains and deformation in the H-connector

4.4.1 Strain distributions

Figure 10 shows the distribution of normal (vertical) strain in the H-connector flanges, from the tension left end (0 mm) to the compression right end (1200 mm).

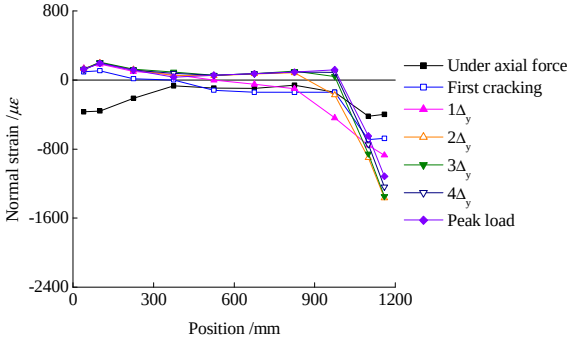

(a) Specimen WH-r1

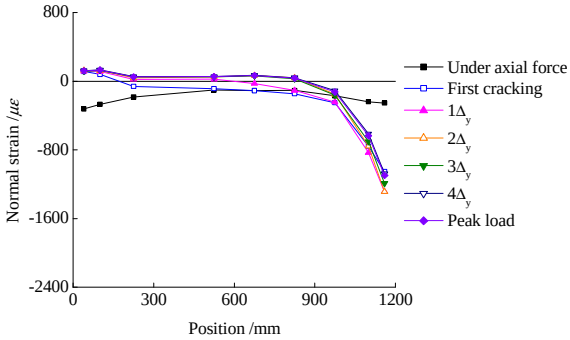

(b) Specimen WH-r2

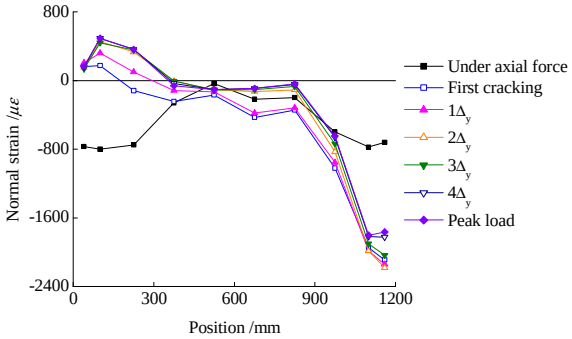

(c) Specimen WH-r3

Figure 10 Normal strain distribution in H-connector

The following may be observed:

(1) On the whole, the compression strain was far larger than the tension strain in H-connector flange, due apparently to the combined axial compression and bending effect. To be specific, when the lateral load reached the peak load the compression strain (about 1800$\mu\varepsilon$) in the 3-mm-thick HSC flange in specimen WH-r3 was approximately 1.6 times that (about 1100$\mu\varepsilon$) in the 6-mm-thick HSC in the other two specimens.

(2) At the initial loading stage, the H-connector flanges were entirely under compression, and the compressive strain at both ends was larger than that in the middle zone, and this could be due to the fact that bolts were arranged more densely at the ends and thus transferred larger forces than in the middle zone. The initial compression strain at both ends of the H-connector flange in specimen WH-r3 is about twice that in specimens WH-r1 and WH-r2 (700~800$\mu\varepsilon$ vs. 300~400$\mu\varepsilon$). This is because the thickness of H-connector flange in specimen WH-r3 was half of that in the other two specimens, while the axial forces being transferred by the H-connector in the three specimens were nearly the same.

(3) With increasing the lateral load and top displacement, a tensile zone gradually emerged and expanded in the H-connector flange. When the lateral load increased to the peak load, the distances from the neutral axis to the tension end within the H-connector flange in the three specimens were all in the range of 800 ~ 1000 mm, which is in line with the neutral axis in the precast shear wall mentioned above. The occurrence of buckling in the H-connector flange in specimen WH-r3 seemed to have resulted in a larger compression zone in the H-connector than those in the other two specimens.

4.4.2 Strain vs. displacement relationship

The strains near the tension and compression ends in the H-connector flange are plotted versus the increasing top displacement to provide another perspective of the transfer of forces through the H-connector at different stages of the responses. Figure 11 shows the relationship curves for measuring points Y1 and Y2 located near the tension end and points Y9 and Y10 located near the compression end for the three specimens, respectively.

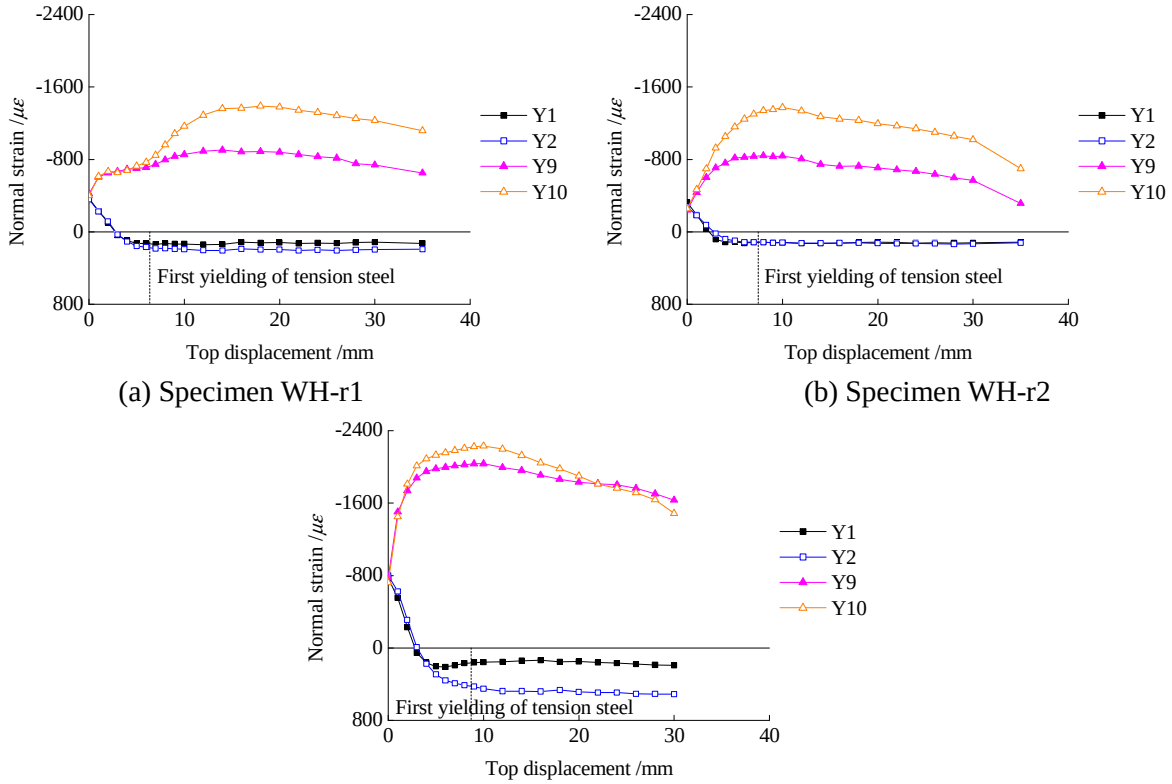

(a) Specimen WH-r1

(b) Specimen WH-r2

(c) Specimen WH-r3

Figure 11 Normal strain-top displacement curve

All curves exhibit a similar pattern in that the strains on the compression end were much larger than the strains on the tension end, for reasons explained earlier. Besides, all strains tend to have experienced a similar process such that at early stage of loading, the strains increased with the increase of the top displacement, but after yielding of the shear wall the strains in the H-connector also flattened, indicating that the transfer of the forces through the H-connector stabilised. Finally the strains in the H-connector decreased which was in line with the degradation of the strength of the shear wall beyond the peak load (see Figure 8).

This implies that the demand on the force transfer through the H-connector may reasonably be determined from an analysis of the wall section corresponding to the peak load.

5 Finite element analysis

5.1 FE model

5.1.1 General considerations

To assist in the interpretation of the experimental phenomena and enable further parametric investigation, finite element (FE) analysis was conducted using ABAQUS software package. The FE model involved several complex mechanical problems such as contact and sliding/friction at bolted connections, in addition to modelling of the concrete and steel materials. Figure 12 shows the FE model of specimen WH-r1. The FE models of the other two specimens are similar to that of WH-r1.

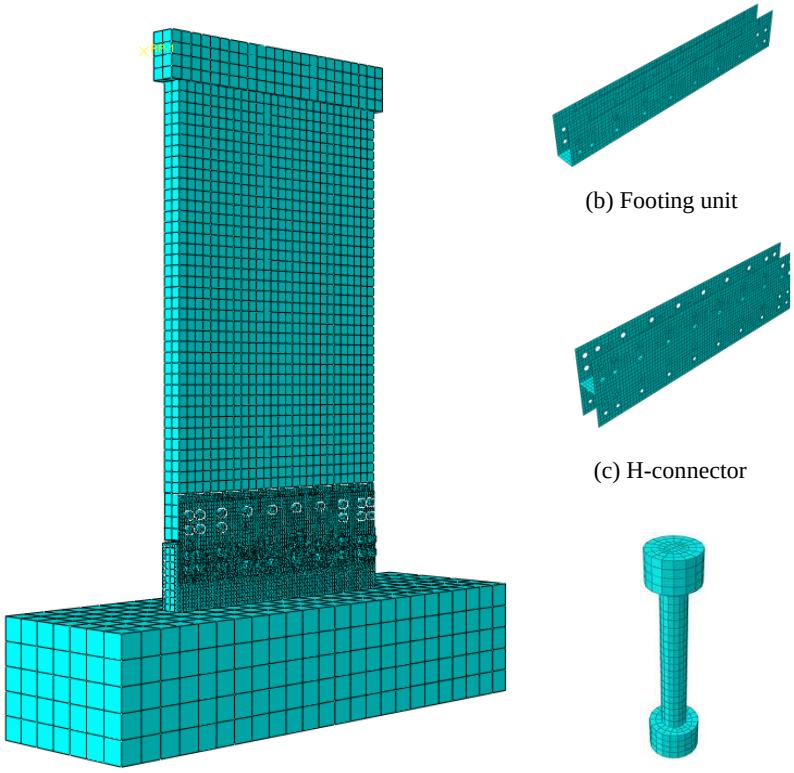

(a) Whole model

(b) Footing unit

(c) H-connector

(d) High strength bolt

Figure 12 Overall configuration and connecting components of FE model

5.1.2 Element types and sizes

The H-connector and the wall footing unit are simulated using 4-node shell elements (S4R). The concrete wall, as well as individual bolts, is simulated using 8-node solid elements (C3D8R). The steel bars are simulated using 2-node truss elements (T3D2).

Since the response of interest is within the plane of the wall, the concrete wall was meshed with two elements through its thickness, and this defines the basic element size of about 45 mm for the main wall. The sizes of C3D8R elements simulating M12, M16, and M22 bolts are approximately 5 mm, 5 mm, and 8 mm, respectively. The size of S4R elements simulating the steel plates of the H-connector and the wall footing unit is 16 mm. The size of the T3D2 elements simulating steel bars is 35 mm. A mesh convergence study was performed and it was confirmed that the chosen mesh density was adequate in ensure sufficient accuracy with reasonable computational time.

5.1.3 Material modelling

In the current FE model, the damage plasticity model available in the ABAQUS library was used for modeling concrete material. This model assumes non-associated potential flow rule and adopts a yield surface to account for the different evolution of strength under tension and compression (Lubliner *et al.*, 1989; Lee and Fenves, 1998). The plastic behavior is generated by the model based on an equivalent uniaxial stress-strain relationship of the concrete. The elasticity modulus (E_c) and Poisson's ratio (v_c) are assumed to be $10^5 \Big/ \left(2.2 + \frac{34.7}{f_{cu}}\right)$ (f_{cu} is the measured compressive strength of the standard concrete cubes) and 0.2, respectively, according to the Chinese code GB50010-2010 (CMC, 2010).

The steel material for steel bars, bolts, H-connector, and the wall footing unit is modelled using a bilinear model. The elasticity modulus (E_s) and Poisson's ratio (v_s) are assumed to be 2.06×10^5 N/mm^2 and 0.3, respectively.

5.1.4 Contact surface and boundary conditions

A surface-based interaction is used to simulate the interface between the H-connector and the wall footing unit, as well as the interface between the bolts and bolt holes. A “hard” contact is applied in the normal direction which allows the two contact surfaces to separate from but not to penetrate into each other, whereas in the tangential direction a Mohr-Coulomb friction model is adopted by assigning a certain frictional coefficient. A frictional coefficient of 0.3 is adopted considering the steel surface to surface contact. The tightening force in the bolts is applied using the “bolt load” function. In the numerical model, the steel bars are all embedded in the concrete neglecting any interface slip; it is worth noting that in this simplified treatment the effect of bond failure would still get represented through failure in the concrete surrounding the steel bars.

The bottom of the base foundation is restrained in all degrees of freedom. The constant vertical load on the top beam is applied prior to the lateral load.

5.2 Verification of FE model

Figure 13 compares the experimental lateral load versus top displacement curves with the simulated results for the three specimens. The comparison demonstrates generally good agreement between the experimental and simulated results. It is interesting to note that in all FE models there is an apparent sudden increase in the lateral displacement at a certain point during loading, whereas in the experimental curves there is not such an abrupt change. This discrepancy may be attributed to the slip at the bolted contact interfaces. In the FE model all bolts are positioned at the centre of the bolt holes in a uniform manner; consequently when slip occurs it would only come to a halt when essentially all bolts come into contact with the inner surface of the bolt holes. On the contrary, the relative position of bolts to their individual host holes in the actual test specimens is understandably random, therefore when slip started individual bolts would have come into contact with the bolt holes in a progressive manner, resulting in a gradual increase of the slip without any sudden change.

Specimen WH-r2 had M12 bolts with a lower pre-tension force of 55 kN as compared to M16 bolts with a pre-tension force of 100 kN in the other two specimens. This explains why the slip occurs much earlier in the FE model for WH-r2 than the other two cases.

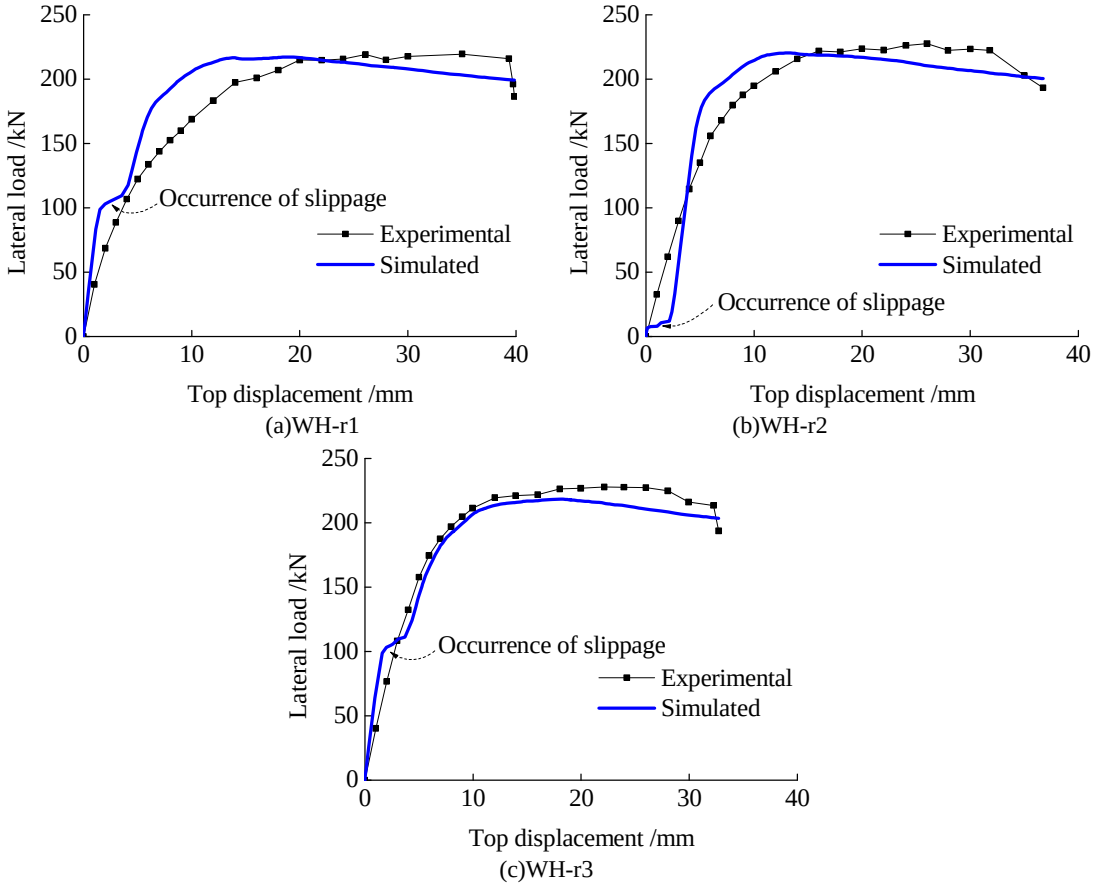

Figure 13 Comparisons of load-displacement curves

Figure 14 shows representative deformation, Mises stress, and plastic strain in the concrete wall at the verge of failure in WH-r1. The results depict a bending-dominated deformation pattern with crushing of concrete at the compression corner of the wall, and this agrees well with the test results. The FE predicted failure modes in the other cases are similar to that of specimen WH-r1.

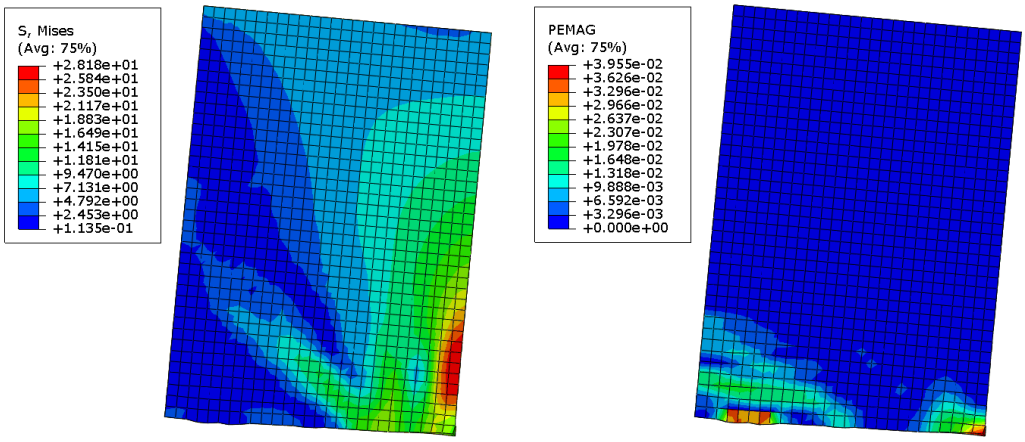

(a) Deformation and mises stress (b) Plastic strain magnitude

Figure 14 Stress and strain distribution in concrete wall

5.3 Deformation and stress in bolts

Figure 15 shows the deformation and stress in the bolts, with a uniform deformation scale factor of 10, at both ends of the specimens when they failed. The deformation in the bolts in WH-r2 is markedly larger than that in the other two specimens, and this agrees well with the inspection of the conditions of the bolts after the experiments, as mentioned in Section 4.1.2.

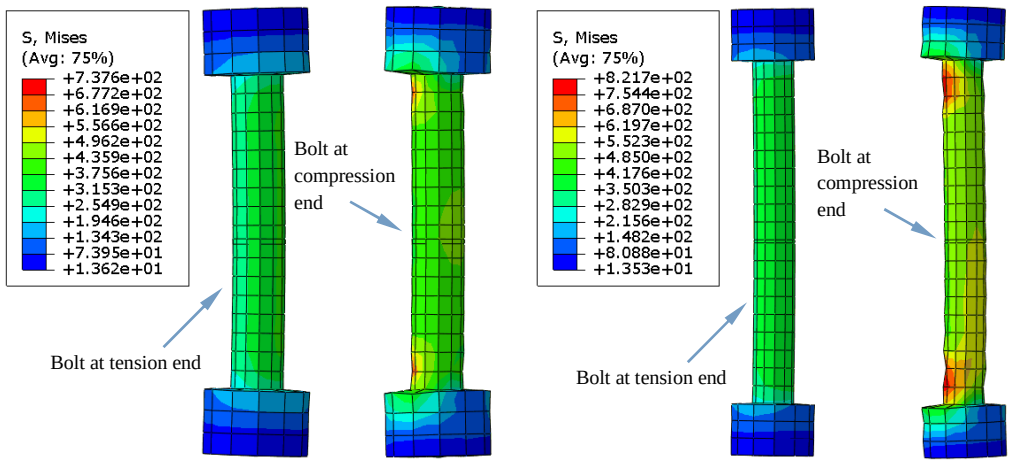

(a) Specimen WH-r1 (b) Specimen WH-r2

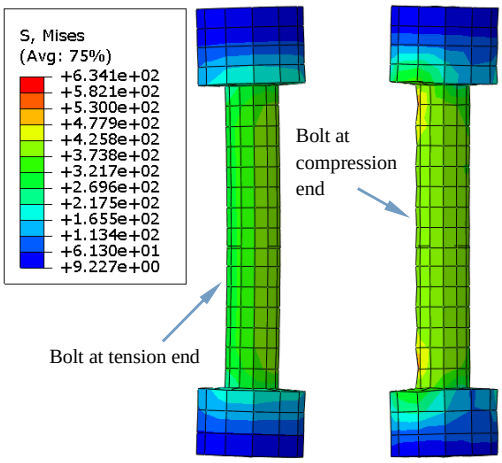

(c) Specimen WH-r3

Figure 15 Deformation and stress in bolts

5.4 Wall bottom end to H-connector interaction

During the course of response the initial gap between the wall bottom end and the web plate of the H-connector will tend to close on the compression side. The degree of the interaction can be examined from the contact opening parameter (COPEN in ABAQUS) of the FE results; a positive value indicates an open state and a value equal or close to 0 indicates occurrence of contact. Figure 16 shows the opening parameter distribution between the wall bottom face and the H-connector web plate when the response reaches failure.

It can be observed that WH-r2 has the largest contact area at compression end whereas WH-r1 has the smallest. This can be explained by the fact that the frictional resistance on the contact surface in WH-r2 is much smaller than that in specimen WH-r1 due to a smaller bolt pre-tension, resulting in earlier slipping. A little larger contact area in WH-r3 than in WH-r1 may be attributed to buckling in the of H-connector in WH-r3.

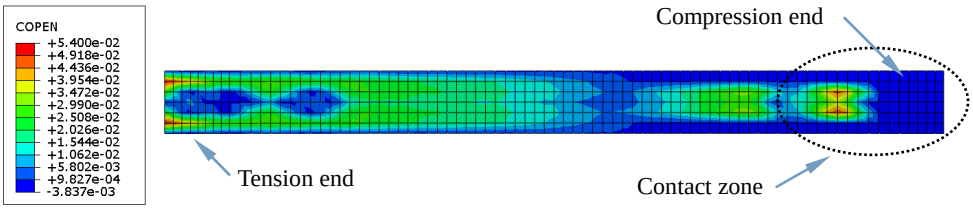

(a) Specimen WH-r1

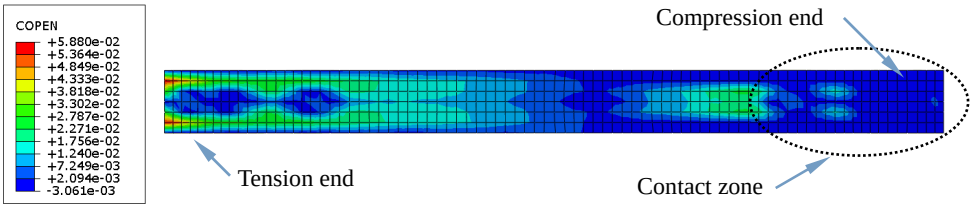

(b) Specimen WH-r2

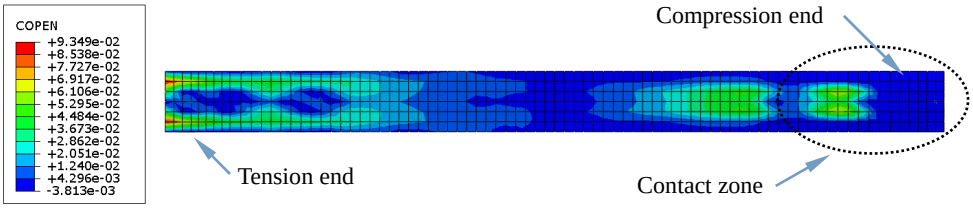

(c) Specimen WH-r3

Figure 16 Contact status on the H-connector web plate

6 Conclusions

This paper presents an experimental study on the lateral load behaviour of a precast shear wall design with horizontal connection, supported by finite element simulation. Three wall-connector assembly specimens were tested to failure under lateral load while subjected to constant vertical compression. The finite element model incorporates detailed connection mechanisms including contact interfaces and pre-tensioning of bolts. Based on the experimental and numerical results, the following conclusions can be drawn:

(1) The horizontally-connected shear wall assemblies exhibited desirable response in terms of ensuring effective load transfer through the connection. The failure mode and ultimate strength in all three cases were governed by the resistance of the main wall, while the H-connector remained largely intact. Buckling within the H-connector in the thinner flange case (WH-r2) indicated a limit state for which the design of the H-connector should consider; however this did not lead to a major problem in the overall response as the load transfer shifted to a contact mechanism on the compression side of the connection.

(2) All assembly specimens demonstrated good ductility performance with displacement ductility factors ranging from 3.7 to 6.2, thanks to the ductile performance of the wall itself and the effective connection. The strain data measured from the H-connector indicated that the load transfer followed closely the response patterns at the critical (bottom) region of the

wall; much larger load transfer occurred in the compression end in a narrow area as opposed to lower and more evenly distributed load transfer towards the tension end.

(3) The friction mechanism alone appeared to be insufficient in providing the necessary load transfer through the connection, and this was particularly the case when the bolt diameter and thereby the pre-tensioning force were smaller (the case of WH-r2). Consequently, the load transfer in the later stage of the response would reply on the bearing resistance of the bolts in the tension region, and bearing and direct compression transfer on the compression side. The friction and bolt bearing capacity meeting the requirement of the tension force transfer in the tensile region of the wall thus becomes a governing condition for the design of the bolts in such a horizontal bolted connection for a precast shear wall.

(4) The finite element model with description of the connection mechanisms proves to represent well the actual behaviour of the shear wall assembly. The FE analysis results confirmed the load transfer mechanisms, the occurrence of slipping at different stages of response in different specimens, and the final failure mode. The FE model can subsequently be employed to conduct further parametric investigations.

The present study has been confined to the general behaviour and working mechanisms within the proposed basic shear wall assembling scheme. There is clearly scope for optimising the H-connector design in order to reduce the amount of steel required, for example the current continuous H-connector across the wall width may be replaced by several short H-connectors. The possibility of filling up the assembling gap between the bottom of a wall panel and the H-connector, so as to eliminate an uncertain factor, may also be examined.

Acknowledgements

The research reported in the paper was part of the Project (2012BAJ14B02) supported by the National Science and Technology Pillar Program during the 12th Five-Year Plan Period.

References

Belleri A, Schoettler MJ, Restrepo JI, Fleischman RB. 2014. Dynamic behavior of rocking and hybrid

cantilever walls in a precast concrete building. *ACI Structural Journal* **111**(3): 661-671.

Bora C, Oliva MG, Nakaki SD, Becker R. 2007. Development of a precast concrete shear-wall system requiring special code acceptance. *PCI Journal* **52**(1): 122-135.

Bournas DA, Negro P, Molina FJ. 2013. Pseudodynamic tests on a full-scale 3-storey precast concrete building: Behavior of the mechanical connections and floor diaphragms. *Engineering Structures* **57**: 609-627.

Choi HK, Choi YC, Choi CS. 2013. Development and testing of precast concrete beam-to-column connections. *Engineering Structures* **56**: 1820-1835.

CMC. 2010. Code for Design of Concrete Structures (GB50010-2010). China Ministry of Construction, China Architecture and Building Press: Beijing, China. (in Chinese)

Henry RS, Brooke NJ, Sritharan S, Ingham JM. 2012. Defining concrete compressive strain in unbonded post-tensioned walls. *ACI Structural Journal* **109**(1): 101-112.

Jiang HB, Chen ZX, Zhang JQ, Wu B, Tian YB, Liu WQ. 2011. Quasi-static test of precast reinforced concrete shear wall structure. *Journal of Building Structures* **32**(6): 34-40. (in Chinese)

Ju SH, Fan CY, Wu GH. 2004. Three-dimensional finite elements of steel bolted connections. *Engineering Structures* **26**(3): 403-413.

Kurama Y, Pessiki S, Sause R, Lu L. 1999. Seismic behavior and design of unbonded posttensioned precast concrete walls. *PCI Journal* **44**(3): 72-89.

Kurama YC. 2002. Hybrid post-tensioned precast concrete walls for use in seismic regions. *PCI Journal* **47**(5): 36-59.

Lee J, Fenves GL. 1998. Plastic-damage model for cyclic loading of concrete structures. *Journal of Engineering Mechanics* **124**(8): 892-900.

Lu XL, Yang JH. 2015. Seismic behavior of T-shaped steel reinforced concrete shear walls in tall buildings under cyclic loading. *The Structural Design of Tall and Special Buildings* **24**(2): 141-157.

Lubliner J, Oliver J, Oller S, Onate E. 1989. A plastic-damage model for concrete. *International Journal of Solids and Structures* **25**(3): 299-326.

Negro P, Bournas DA, Molina FJ. 2013. Pseudodynamic tests on a full-scale 3-storey precast concrete building: Global response. *Engineering Structures* **57**: 594-608.

Pall AS, Marsh C, Fazio P. 1980. Friction joints for seismic control of large panel structures. *PCI Journal* **25**(6): 38-61.

Park R. 1989. Evaluation of ductility of structures and structural assemblages from laboratory testing. *Bulletin of the New Zealand National Society for Earthquake Engineering* **22**(3): 155-166.

Pavese A, Bournas DA. 2011. Experimental assessment of the seismic performance of a prefabricated concrete structural wall system. *Engineering Structures* **33**(6): 2049-2062.

Pekau OA, Hum D. 1991. Seismic response of friction jointed precast panel shear walls. *PCI Journal* **36**(2): 56-71.

Perez FJ, Pessiki S, Sause R. 2013. Experimental lateral load response of unbonded post-tensioned precast concrete walls. *ACI Structural Journal* **110**(6): 1045-1055.

Perez FJ, Sause R, Pessiki S. 2007. Analytical and experimental lateral load behavior of unbonded posttensioned precast concrete walls. *Journal of Structural Engineering* **133**(11): 1531-1540.

Qian JR, Yang XK, Qin H, Peng YY, Zhang JM, Li JS. 2011. Tests on seismic behavior of pre-cast shear walls with various methods of vertical reinforcement splicing. *Journal of Building Structures* **32**(6): 51-59. (in Chinese)

Shemie M. 1973. Bolted connections in large panel system buildings. *PCI Journal* **18**(1): 27-33.

Smith BJ, Kurama YC, McGinnis MJ. 2013. Behavior of precast concrete shear walls for seismic regions: Comparison of hybrid and emulative specimens. *Journal of Structural Engineering* **139**(11): 1917-1927.

Sun J, Qiu HX, Lu B. 2015. Experimental validation of horizontal joints in an innovative totally precast shear wall system. *Journal of Southeast University (English Edition)* **31**(1): 124-129.

Wang ZJ, Liu WQ, Zhai WH, Li XM, Xu QF, Wang Y. 2015. Experimental study on seismic behavior of new type reinforced concrete composite shear wall. *Journal of Central South University (Science and Technology)* **46**(4): 1409-1419. (in Chinese)

Zhang HM, Lu XL, Duan YF, Li JB. 2011. Experimental study and numerical simulation of partially prefabricated laminated composite RC walls. *Advances in Structural Engineering* **14**(5): 967-979.